INL/RPT-22-68240

Improvement of Closures and Mechanistic Limit Modeling in Sockeye

July 2022

J. E. Hansel[1]

[1]Idaho National Laboratory

INL is a U.S. Department of Energy National Laboratory
operated by Battelle Energy Alliance, LLC

INL/RPT-22-68240

Improvement of Closures and Mechanistic Limit Modeling in Sockeye

J. E. Hansel[1]

[1]**Idaho National Laboratory**

July 2022

Idaho National Laboratory
Computational Frameworks Department
Idaho Falls, Idaho 83415

http://www.inl.gov

Prepared for the
U.S. Department of Energy
Office of Nuclear Energy
Under DOE Idaho Operations Office
Contract DE-AC07-05ID14517

Page intentionally left blank

ACKNOWLEDGEMENTS

We would like to thank Dr. Bob Reid and Dr. Katrina Sweetland of Los Alamos National Laboratory for giving us direction and assistance on pressure drop closure development and assessment.

Sockeye development is being carried out under the auspices of Idaho National Laboratory, a contractor of the U.S. Government under contract number DEAC07-05ID14517. Accordingly, the U.S. Government retains a nonexclusive, royalty-free license to publish or reproduce the published form of this contribution, or allows others to do so, for U.S. Government purposes.

Page intentionally left blank

CONTENTS

FIGURES

TABLES

1 INTRODUCTION

Sockeye is an application for the modeling of heat pipes used in nuclear microreactors, based on the Multiphysics Object-Oriented Simulation Environment (MOOSE) framework [1]. The MOOSE framework is a finite element framework written in C++, designed to enable multiphysics coupling [2]. Sockeye's main heat pipe modeling capability is a 1D, two-phase flow model that simulates the interior of the heat pipe (working fluid and wick), which can then be coupled to 2D heat conduction in the cladding. This flow model requires numerous closure relations in addition to the working fluid equation of state, including interfacial and wall heat transfer coefficients, friction factors, and capillary pressure.

One of the primary objectives of a heat pipe modeling capability is to accurately predict and model heat pipe operational limits. Perhaps the most important limit to consider is the capillary limit, which corresponds to the limit of a heat pipe to sustain circulation of the working fluid by capillary action in the wick. If a given power throughput requires a certain mass flow rate of the working fluid, but the total pressure drop corresponding to this mass flow rate exceeds the maximum capillary pressure in the wick, then circulation cannot be sustained, and it eventually results in a local dryout, leading to failure of the heat pipe to transfer heat efficiently. The key to accurately predicting this limit is having accurate closures for the various terms related to pressure drops. This is also true of the viscous limit, which requires that the pressure drop in the vapor phase does not produce a sub-zero pressure. The boiling limit, which occurs when excessive nucleate boiling occurs in the heat pipe, requires accurate wall heat and mass transfer closures. The other considered limits include the sonic limit, which occurs when there is choked flow in the heat pipe, and the entrainment limit, due to excessive shearing of the liquid from the wick surface.

This report discusses improvements made to Sockeye's closures and its ability to model heat pipe limits mechanistically and is organized as follows. Section 2 discusses the various improvements made to Sockeye in this work, Section 3 discusses some results of these improvements, and Section 4 gives our conclusions about this work.

2 IMPROVEMENTS

2.1 Closures System

Numerous alternative heat pipe model closures exist. Generally, there is no universal set of closures for heat pipes, since closures largely depend on the heat pipe wick design and working fluid. Furthermore, many heat pipe designs are proprietary, precluding any inclusion of corresponding closures directly in Sockeye. For this reason, the `Closures` system was developed. This is a pluggable system that allows for the addition of new closures classes, and also it allows users to fully customize their utilized closures classes.

In an input file, there is now a `Closures` syntax block, which can be used as follows to create a closures object and pass it to the `HeatPipe3Phase` component via the new `closures` parameter:

```
[Closures]
  [my_closures]
    type = Closures3Phase
    ...
  []
[]
```

```
[Components]
  [my_hp]
    type = HeatPipe3Phase
    ...
    closures = my_closures
  []
[]
```

In the case of multiple `HeatPipe3Phase` components, the same closures object may be used for all. In the sections that follow, various new closures are introduced, which often are added alongside existing closure models with a corresponding parameter to `Closures3Phase` added to switch between models.

2.2 Interfacial Heat Transfer Coefficients

An interfacial heat transfer occurs between each phase and the interface; this heat flux is modeled as a convective heat flux:

$$q_k^{\text{int}} = \mathcal{H}_k^{\text{int}}(T_{\text{int}} - T_k)\,, \tag{1}$$

where q_k^{int} is the heat flux to phase k from the interface, $\mathcal{H}_k^{\text{int}}$ is the interfacial heat transfer coefficient for phase k, T_{int} is the interface temperature, and T_k is the temperature of phase k.

Carey [3] developed a simplified form of the net heat flux across a liquid-vapor interface using the kinetic theory of gases, assuming small relative pressure and temperature differences across the phases [4]:

$$q_{\text{int}} = \mathcal{H}_{\text{int}}(T_\ell - T_v)\,, \tag{2}$$

$$\mathcal{H}_{\text{int}} = \left(\frac{2\alpha}{2-\alpha}\right)\left(\frac{h_{\ell v}^2}{T_v v_{\ell v}}\right)\sqrt{\frac{M_v}{2\pi R_u T_v}}\left(1 - \frac{p_v v_{\ell v}}{2h_{\ell v}}\right)\,, \tag{3}$$

where

- q_{int} is the total heat flux from the liquid and vapor phases to the interface (positive for evaporation, negative for condensation)
- α is an accommodation coefficient
- $h_{\ell v} = h_v - h_\ell$ is the latent heat of vaporization
- $v_{\ell v} = v_v - v_\ell$ is the difference in specific volume
- M_v is the molar mass of the working fluid
- R_u is the universal gas constant.

The accommodation coefficient varies widely in literature, but for pure, uncontaminated working fluids and interfaces, $\alpha = 1$ may be assumed [4].

Comparing Carey's formulation to Equation (1),

$$\mathcal{H}_{\text{int}}(T_\ell - T_v) = \mathcal{H}_\ell^{\text{int}}(T_\ell - T_{\text{int}}) + \mathcal{H}_v^{\text{int}}(T_v - T_{\text{int}})\,. \tag{4}$$

Unfortunately, there is no direct definition for $\mathcal{H}_\ell^{\text{int}}$ and $\mathcal{H}_v^{\text{int}}$ based on this comparison, since Carey's formulation does not consider an interfacial temperature; thus, some simplification is required. The most straightforward simplification is assuming $\mathcal{H}_\ell^{\text{int}} = \mathcal{H}_v^{\text{int}}$. If additionally, the vapor phase is assumed to be at the saturation state ($T_v \approx T_{\text{int}}$), which is found to be approximately true in practice, the phasic interfacial heat transfer coefficients match the interfacial heat transfer coefficient defined by Equation (3):

$$\mathcal{H}_\ell^{\text{int}} = \mathcal{H}_v^{\text{int}} = \mathcal{H}_{\text{int}} = \left(\frac{2\alpha}{2-\alpha}\right)\left(\frac{h_{\ell v}^2}{T_v v_{\ell v}}\right)\sqrt{\frac{M_v}{2\pi R_u T_v}}\left(1 - \frac{p_v v_{\ell v}}{2h_{\ell v}}\right) . \tag{5}$$

Here we take the following definitions:

$$T_v = T_{\text{int}} , \tag{6}$$

$$h_{\ell v} = h_v^{\text{int}} - h_\ell^{\text{int}} , \tag{7}$$

$$v_{\ell v} = v_v(\bar{p}_{\text{int}}, T_{\text{int}}) - v_\ell(\bar{p}_{\text{int}}, T_{\text{int}}) , \tag{8}$$

$$p_v = \bar{p}_{\text{int}} . \tag{9}$$

2.3 Wall Heat Transfer

The total wall heat flux into a heat pipe, q_{wall}, is partitioned into a number of terms:

$$q_{\text{wall}} = q_{\text{wall},\ell sw}^{\text{conv}} + q_{\text{wall},\ell sw}^{\text{boil}} + q_{\text{wall},v} , \tag{10}$$

where $q_{\text{wall},\ell sw}^{\text{conv}}$ is the heat flux from the wall to the liquid-solid-wick phase:

$$q_{\text{wall},\ell sw}^{\text{conv}} = (1 - f_{\text{boil}})\mathcal{H}_{\text{wall},\ell sw}(T_{\text{wall}} - T_{\ell sw})\kappa_{\ell sw} , \tag{11}$$

$q_{\text{wall},\ell sw}^{\text{boil}}$ is the heat flux from the wall into boiling:

$$q_{\text{wall},\ell sw}^{\text{boil}} = f_{\text{boil}}\mathcal{H}_{\text{wall},\ell sw}(T_{\text{wall}} - T_{\ell sw})\kappa_{\ell sw} , \tag{12}$$

and $q_{\text{wall},v}$ is the heat flux from the wall to the vapor phase:

$$q_{\text{wall},v} = \mathcal{H}_{\text{wall},v}(T_{\text{wall}} - T_v)\kappa_v . \tag{13}$$

T_{wall}, $T_{\ell sw}$, and T_v are the wall, liquid-solid-wick, and vapor temperatures, respectively, $\mathcal{H}_{\text{wall},\ell sw}$ and $\mathcal{H}_{\text{wall},v}$ are the wall heat transfer coefficients for the liquid-solid-wick phase and vapor phase, respectively, $\kappa_{\ell sw}$ and κ_v are the wall contact fractions (that sum to one) for liquid-solid-wick and vapor, respectively, and f_{boil} is the fraction of heat flux into liquid-solid-wick phase that participates in boiling.

Wall heat transfer is categorized into a number of regimes, described in the sections that follow.

2.3.1 Vapor

If there is no liquid or solid phase, the vapor phase is assumed to be in full contact with the wall: $\kappa_{\ell sw} = 0$ and $\kappa_v = 1$. The heat transfer coefficient is calculated to be

$$\mathcal{H}_{\text{wall},v} = \text{Nu}_v \frac{k_v}{D_{h,v}} , \tag{14}$$

where Nu_v is the vapor Nusselt number, k_v is the vapor thermal conductivity, and the hydraulic diameter $D_{h,v}$ assumes the vapor phase has a circular cross section:

$$D_{h,v} = 2\sqrt{\frac{\alpha_v A}{\pi}}\,. \tag{15}$$

The Nusselt number is taken from the Skupinski correlation [5]:

$$\mathrm{Nu}_v = 4.82 + 0.0185 \cdot \mathrm{Pe}_v^{0.827}\,, \tag{16}$$

where Pe_v is the vapor Peclet number.

2.3.2 Convection and Film Condensation

If the liquid phase is present, and there is no solid phase, the liquid phase is assumed to be in full contact with the wall: $\kappa_{\ell sw} = 1$ and $\kappa_v = 0$. If the wall temperature is less than the interface temperature T_{int}, two regimes are considered, based on the volume fractions of each phase:

$$\mathcal{H}_{\mathrm{wall},\ell sw} = \begin{cases} \mathcal{H}^{\mathrm{film}}_{\mathrm{wall},\ell sw} & \alpha_\ell \le \alpha_{\ell,2} \\ (1-f_{\mathrm{film}})\mathcal{H}^{\mathrm{conv}}_{\mathrm{wall},\ell sw} + f_{\mathrm{film}}\mathcal{H}^{\mathrm{film}}_{\mathrm{wall},\ell sw} & \alpha_{\ell,2} < \alpha_\ell < \alpha_{\ell,1} \\ \mathcal{H}^{\mathrm{conv}}_{\mathrm{wall},\ell sw} & \alpha_\ell \ge \alpha_{\ell,1} \end{cases}, \tag{17}$$

where $0 \le f_{\mathrm{film}} \le 1$ is the linear transition coefficient:

$$f_{\mathrm{film}} = \frac{\alpha_\ell - \alpha_{\ell,1}}{\alpha_{\ell,2} - \alpha_{\ell,1}}\,, \tag{18}$$

$$\alpha_{\ell,1} = 1 - \alpha_w - \alpha_v^{\mathrm{wick,o,+}}\,, \tag{19}$$

$$\alpha_{\ell,2} = \frac{1}{2}\alpha_{\ell,1}\,. \tag{20}$$

The convection heat transfer coefficient is computed as

$$\mathcal{H}^{\mathrm{conv}}_{\mathrm{wall},\ell sw} = \mathrm{Nu}_\ell \frac{k_\ell}{D_{h,\ell}}\,, \tag{21}$$

where Nu_ℓ is the liquid Nusselt number, k_ℓ is the liquid thermal conductivity, and the liquid hydraulic diameter $D_{h,\ell}$ definition assumes the liquid phase has an annular cross section with inner diameter D_ℓ, assuming there is no wick:

$$D_\ell = \sqrt{D^2_{\mathrm{clad},i} - \frac{4\alpha_\ell A}{\pi}}\,, \tag{22}$$

where $D_{\mathrm{clad},i}$ is the inner cladding diameter, giving the corresponding hydraulic diameter to be the following:

$$D_{h,\ell} = \frac{4\alpha_\ell A}{\pi(D_\ell + D_{\mathrm{clad},i})}\,. \tag{23}$$

The Nusselt number is again computed using the Skupinski correlation [5]:

$$\mathrm{Nu}_\ell = 4.82 + 0.0185 \cdot \mathrm{Pe}_\ell^{0.827}\,, \tag{24}$$

where Pe_ℓ is the liquid Peclet number.

The film condensation heat transfer coefficient is computed as

$$\mathcal{H}^{\text{film}}_{\text{wall},\ell sw} = \text{Nu}_\ell \frac{k_\ell}{\delta_\ell}\,, \tag{25}$$

where the liquid thickness is computed as

$$\delta_\ell = \max\left(10^{-6}, \frac{D_{\text{clad,i}}}{2}\left(1 - \sqrt{\min(1, 1-\alpha_\ell)}\right)\right)\,. \tag{26}$$

$$\text{Nu}_\ell = \sqrt{\text{Nu}^2_{\ell,\text{lam}} + \text{Nu}^2_{\ell,\text{turb}}}\,, \tag{27}$$

$$\text{Nu}_{\ell,\text{lam}} = 2(1 + 0.000183\text{Re}_\ell)\,, \tag{28}$$

$$\text{Re}_\ell = \frac{\alpha_\ell \rho_\ell |u_\ell| D_{\text{clad,i}}}{\mu_\ell}\,, \tag{29}$$

$$\text{Nu}_{\ell,\text{turb}} = 0.25\text{Nu}_\ell\,, \tag{30}$$

where Nu_ℓ is computed using the Skupinski correlation.

If the wall temperature is greater than the interfacial temperature but less than the onset of nucleate boiling temperature T_{ONB}, the heat transfer coefficient is taken to be equal to $\mathcal{H}^{\text{conv}}_{\text{wall},\ell sw}$.

2.3.3 Nucleate Boiling

The temperature T_{ONB} is the onset of nucleate boiling temperature, which is given by [4]:

$$T_{\text{ONB}} = T_v + \frac{2\sigma T_v}{h_{\ell v}\rho_v}\left(\frac{1}{R_b} - \frac{1}{R_{\text{men}}}\right)\,, \tag{31}$$

where σ is the surface tension, $h_{\ell v}$ is the latent heat of fusion, R_b is the bubble radius, and R_{men} is the meniscus radius. If the wall temperature exceeds this temperature (and liquid is in contact with the wall), nucleate boiling occurs.

The heat transfer coefficient is the sum of the convection coefficient from (21) and the pool boiling heat transfer coefficient:

$$\mathcal{H}_{\text{wall},\ell sw} = \mathcal{H}^{\text{conv}}_{\text{wall},\ell sw} + \mathcal{H}^{\text{PB}}_{\text{wall},\ell sw}(T_{\text{wall}}) - \mathcal{H}^{\text{PB}}_{\text{wall},\ell sw}(T_{\text{ONB}})\,, \tag{32}$$

where the function $\mathcal{H}^{\text{PB}}_{\text{wall},\ell sw}(T)$ is the pool boiling heat transfer coefficient, which is calculated using the correlation from [6]:

$$\mathcal{H}^{\text{PB}}_{\text{wall},\ell sw}(T) = C(T_{\text{wall}} - T)^{0.7} p_r^m\,, \tag{33}$$

where for the reduced pressure $p_r = p_\ell / p_c < 0.001$, $C = 13.7$ and $m = 0.22$, and for $p_r > 0.001$, $C = 6.9$ and $m = 0.12$. When $T_{\ell sw} > T_{\text{wall}}$, $\mathcal{H}^{\text{PB}}_{\text{wall},\ell sw}(T)$ is set to zero.

Lastly, the boiling fraction is computed as follows:

$$f_{\text{boil}} = \frac{\mathcal{H}^{\text{PB}}_{\text{wall},\ell sw}\left(T_{\text{wall}}\right) - \mathcal{H}^{\text{PB}}_{\text{wall},\ell sw}\left(T_{\text{ONB}}\right)}{\mathcal{H}_{\text{wall},\ell sw}}\,. \tag{34}$$

2.4 Vapor Pressure Drop

The vapor momentum balance equation is

$$\frac{\partial \alpha_v \rho_v u_v A}{\partial t} + \frac{\partial \alpha_v (\rho_v u_v^2 + p_v) A}{\partial x} = p_{\text{int}} \frac{\partial \alpha_v}{\partial x} A - F_v^{\text{visc}} A + \alpha_v \rho_v g_x A \,, \tag{35}$$

where F_v^{visc} represents a viscous force density of the form

$$F_v^{\text{visc}} = \frac{f_{D,v} \alpha_v \rho_v |u_v| u_v}{2 D_{h,v}} \,, \tag{36}$$

where $f_{D,v}$ is a Darcy friction factor and $D_{h,v}$ is the hydraulic diameter of the vapor. Assuming steady flow and negligible volume fraction gradient ($\frac{\partial \alpha_v}{\partial x} \approx 0$), the momentum balance equation is manipulated to give the steady-state pressure gradient:

$$\frac{\partial p_v}{\partial x} = -\frac{f_{D,v} \rho_v |u_v| u_v}{2 D_{h,v}} - \frac{\partial \rho_v u_v^2}{\partial x} + \rho_v g_x \,. \tag{37}$$

The first term on the right side represents the viscous pressure gradient, and the second term represents the inertial pressure gradient, which are discussed in Sections 2.4.1 and 2.4.2, respectively.

Closures in general depend on two main parameters: the axial Reynolds number and the radial Reynolds number. The axial Reynolds number is defined as

$$\text{Re}_{x,v} = \frac{\rho_v u_v D_v}{\mu_v} \,, \tag{38}$$

where D_v is the diameter of the vapor channel. The radial Reynolds number is defined as

$$\text{Re}_{r,v} = \frac{\rho_v w_v R_v}{\mu_v} \,, \tag{39}$$

where w_v is the radial vapor velocity and R_v is the radius of the vapor channel. Note that it is customary to use the vapor radius as the reference length in the radial Reynolds number, whereas, for the axial Reynolds number, the vapor diameter is customary [7]. The radial vapor velocity is estimated from the interfacial mass flux Γ_{int} from the liquid to the vapor. The interfacial mass flux can be expressed in terms of the radial vapor velocity:

$$\Gamma_{\text{int}} = \rho_v w_v \,. \tag{40}$$

Therefore,

$$\text{Re}_{r,v} = \frac{\Gamma_{\text{int}} R_v}{\mu_v} \,. \tag{41}$$

Note that this definition gives a positive value for evaporation and negative value for condensation.

2.4.1 Viscous Vapor Pressure Drop

The viscous pressure gradient is assumed to be of the form

$$\left.\frac{\partial p_v}{\partial x}\right|^{\text{visc}} = -\frac{f_{D,v} \rho_v |u_v| u_v}{2 D_{h,v}} \,, \tag{42}$$

with the Darcy friction factor $f_{D,v}$ determined by closures. Sockeye adopts the closures used in the steady-state heat pipe analysis code HTPIPE [8].

For $\Gamma_{\text{int}} \geq \epsilon$ (as is typical in the evaporator section), the mass addition stabilizes the vapor flow, and thus the flow is assumed to be laminar for all Reynolds numbers, so Hagen-Poiseuille flow applies, but Busse uses a semi-empirical correction to account for the deviation of the velocity profile from the parabolic profile assumed by Hagen-Poiseuille equations [9]:

$$f_{D,v} = \frac{64}{\text{Re}_{x,v}} \left(1 + \frac{2}{3}a\right) , \tag{43}$$

where a is the following function of radial Reynolds number [4, 8]:

$$a = \frac{15}{22} \left(5 + \frac{18}{\text{Re}_{r,v}} - \sqrt{\left(5 + \frac{18}{\text{Re}_{r,v}}\right)^2 - \frac{44}{5}}\right) . \tag{44}$$

For $\Gamma_{\text{int}} < \epsilon$ (as is typical in the adiabatic and condenser sections), turbulence may occur, and thus other relations are incorporated [8]:

$$f_{D,v} = \begin{cases} \frac{64}{\text{Re}_{x,v}} & \text{Re}_{x,v} \leq 2000 \\ \frac{0.316}{\text{Re}_{x,v}^{0.25}} & 2000 < \text{Re}_{x,v} \leq 20000 \\ \frac{0.184}{\text{Re}_{x,v}^{0.2}} & \text{Re}_{x,v} > 20000 \end{cases} . \tag{45}$$

To alleviate possible convergence difficulties associated with closure discontinuities, smooth transitions are implemented between the different relations.

Figure 1 shows the vapor friction factor vs. axial Reynolds number, for several radial Reynolds number values. Note the smooth transitions at $\text{Re}_{x,v} = 2,000$ and $\text{Re}_{x,v} = 20,000$.

2.4.2 Inertial Vapor Pressure Drop

The inertial pressure gradient term

$$\left.\frac{\partial p_v}{\partial x}\right|^{\text{iner}} = -\frac{\partial \rho_v u_v^2}{\partial x} \tag{46}$$

does not yield the correct inertial pressure drops in practice, due to corrections that need to be made for the radial velocity distribution, since a one-dimensional treatment cannot directly capture these effects [10]. Correcting this term by a factor f_{iner}, hereafter referred to as the "inertial fraction," gives

$$\left.\frac{\partial p_v}{\partial x}\right|^{\text{iner}} = -f_{\text{iner}} \frac{\partial \rho_v u_v^2}{\partial x} . \tag{47}$$

Various empirical or analytic models attempt to predict this fraction. To integrate this correction into Sockeye's equations, we add a source term to the vapor momentum equation:

$$\frac{\partial \alpha_v \rho_v u_v A}{\partial t} + \frac{\partial \alpha_v (\rho_v u_v^2 + p_v) A}{\partial x} = p_{\text{int}} \frac{\partial \alpha_v}{\partial x} A - F_v^{\text{visc}} A + \alpha_v \rho_v g_x A + (1 - f_{\text{iner}}) \frac{\partial \alpha_v \rho_v u_v^2 A}{\partial x} . \tag{48}$$

Instead of treating this term as a flux term as on the left side, which would complicate the numerical flux computation, this term will be treated as a volumetric source term by approximating the gradient as follows.

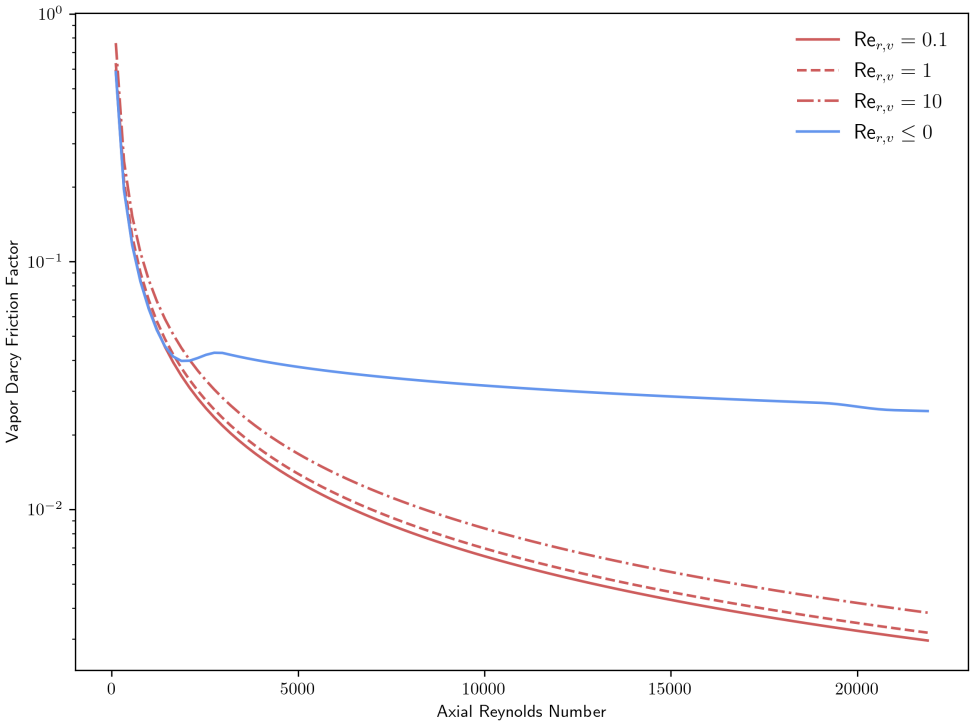

Figure 1: Vapor friction factor at various axial and radial Reynolds numbers.

Assuming steady flow, negligible volume fraction gradient ($\frac{\partial \alpha_v}{\partial x} \approx 0$), and negligible vapor density gradient ($\frac{\partial \rho_v}{\partial x} \approx 0$), the vapor continuity equation gives

$$\alpha_v \rho_v \frac{\partial u_v}{\partial x} A = \Gamma_{\text{int}} a_{\text{int}} A \,. \tag{49}$$

Then

$$(1 - f_{\text{iner}}) \frac{\partial \alpha_v \rho_v u_v^2 A}{\partial x} \approx 2(1 - f_{\text{iner}}) \alpha_v \rho_v u_v \frac{\partial u_v}{\partial x} A \approx 2(1 - f_{\text{iner}}) \Gamma_{\text{int}} u_v a_{\text{int}} A \,. \tag{50}$$

Thus the resulting momentum equation is

$$\frac{\partial \alpha_v \rho_v u_v A}{\partial t} + \frac{\partial \alpha_v (\rho_v u_v^2 + p_v) A}{\partial x} = p_{\text{int}} \frac{\partial \alpha_v}{\partial x} A - F_v^{\text{visc}} A + \alpha_v \rho_v g_x A + 2(1 - f_{\text{iner}}) \Gamma_{\text{int}} u_v a_{\text{int}} A \,. \tag{51}$$

Now we discuss the computation of f_{iner}. For $\Gamma_{\text{int}} \geq \epsilon$ (as is typical in the evaporator section), the following inertial fraction is used, based on the work by Busse [8, 9]:

$$f_{\text{iner}} = \frac{4}{3} \left(1 - \frac{a}{6} + \frac{2a^2}{45} \right) , \tag{52}$$

where a is computed as in Equation (44).

For $\Gamma_{\text{int}} < \epsilon$, Busse's theory computes a spatially-varying coefficient a that requires a nonlinear solve at each point. Furthermore, Busse's theory is only valid for $\mathrm{Re}_{r,v} > -2.25$. To avoid these complications, in the adiabatic section and condenser, Sockeye simply assumes $a = 0$, which corresponds to a parabolic profile. Thus,

$$f_{\text{iner}} = \frac{4}{3}\,. \tag{53}$$

2.5 Liquid Pressure Drop

When the wick structure is not flush to the inner cladding surface, there are potentially two flow paths for the liquid to travel back from the condenser region to the evaporator region: the wick and the annulus. For flow through the wick structure, the wick permeability is the relevant closure, while for flow through the annular gap, a friction factor is the relevant closure. If the user does not provide a friction factor for the liquid phase, then the friction factor is determined assuming laminar flow in the annulus. Reference [11] gives the following closure:

$$f_{\text{D}} = \frac{24}{\text{Re}} \left(\frac{D_{\text{wick,o}}}{D_{\text{hp,i}}} \right)^{0.035}\,, \tag{54}$$

while the Hagen-Poiseuille theory for fully developed flows for a concentric annulus gives the following friction factor [10]:

$$f_{\text{D}} = \frac{64}{\text{Re}}\zeta\,, \tag{55}$$

$$\zeta \equiv \frac{(a-b)^2(a^2-b^2)}{a^4 - b^4 - \frac{(a^2-b^2)^2}{\ln(a/b)}}\,, \tag{56}$$

where a and b are the outer and inner radii of the channel, here, $R_{\text{clad,i}}$ and $R_{\text{wick,o}}$, respectively. Note that, for $a \approx b$, $\zeta = \frac{3}{2}$.

If the liquid flows entirely through the annular gap, pressure losses are determined from a friction factor as follows:

$$\frac{dp_\ell}{dx} = -\frac{1}{2} f_{\text{D},\ell} \frac{\rho_\ell |u_{\ell,\text{ann}}| u_{\ell,\text{ann}}}{D_{\text{h,ann},\ell}}\,, \tag{57}$$

where $u_{\ell,\text{ann}}$ is the velocity of the liquid phase if the entire mass flow rate goes through the annular gap:

$$u_{\ell,\text{ann}} \equiv u_\ell \frac{\alpha_\ell A}{A_{\ell,\text{ann}}}\,, \tag{58}$$

$$A_{\ell,\text{ann}} \equiv \min(\alpha_\ell A, A_{\text{ann}})\,, \tag{59}$$

and $D_{\text{h,ann},\ell}$ is the hydraulic diameter corresponding to $A_{\ell,\text{ann}}$, the liquid annulus, which has a maximum thickness of the annular gap thickness:

$$D_{\text{h,ann},\ell} = 2\min(\delta_\ell, \delta_{\text{ann}})\,, \tag{60}$$

$$\delta_{\text{ann}} \equiv R_{\text{clad,i}} - R_{\text{wick,o}}\,, \tag{61}$$

$$\delta_\ell \equiv R_{\text{clad,i}} - R_\ell \,, \tag{62}$$

$$R_\ell \equiv \sqrt{R_{\text{clad,i}}^2 - \frac{\alpha_\ell A}{\pi}} \,. \tag{63}$$

The source term corresponding to Equation (57) is

$$-F_\ell A \equiv -\frac{1}{2} f_{\text{D},\ell} \frac{\rho_\ell |u_{\ell,\text{ann}}| u_{\ell,\text{ann}}}{D_{\text{h,ann},\ell}} A_{\ell,\text{ann}} \,. \tag{64}$$

2.6 Slope Reconstruction

The spatial discretization in Sockeye is a Godunov-type finite volume scheme adapted from Reference [12]. The key ingredient of this scheme is in the evaluation of numerical flux terms between each pair of elements: $f(\mathbf{U}_L, \mathbf{U}_R)$. Sockeye uses a two-phase extension of the HLLC Riemann solver. The Godunov scheme evaluates this flux with the cell center solutions of the adjoining cells, yielding first-order accuracy: $f(\mathbf{U}_i, \mathbf{U}_{i+1})$. However, if instead the fluxes are evaluated with a linear reconstruction of the solution on each side of the interface, second-order accuracy can be achieved: $f(\tilde{\mathbf{U}}_i, \tilde{\mathbf{U}}_{i+1})$. To prevent spurious oscillations in the presence of strong shocks and discontinuities, the total variation diminishing (TVD) concept is used to develop various slope limitation schemes, which selectively reduce the slopes in the presence of such conditions [13].

3 RESULTS

Pressure drop closures were tested using three cases of a test problem featuring a sodium heat pipe with an annular wick. Results were compared against analytic solutions and HTPIPE [8]. Table 1 summarizes the temperature and power for each of these cases. The value given in the "Temperature" column corresponds to the initial temperature used in the Sockeye simulation, and the value given in the "Power" column is the power uniformly added along the evaporator length and uniformly removed along the condenser length.

Case	Power [W]	Temperature [K]
1	200	800
2	1,000	1000
3	2,500	1200

Table 1: Test cases for sodium heat pipe with annular wick.

Figure 2 shows these cases in relation to analytic approximations to the various operational limits, as well as some closure transition points. The cases were designed such that each of the closure regimes would be used. The line $\text{Re}_{\text{r,cond}} = -2.25$ denotes the condenser radial Reynolds number below which the theory of Busse [9] no longer applies; therefore, Busse's theory can only be applied to Case 1.

HTPIPE was run with the (power, evaporator exit temperature) mode. The evaporator exit temperature was taken from the steady-state Sockeye solution to ensure consistent results.

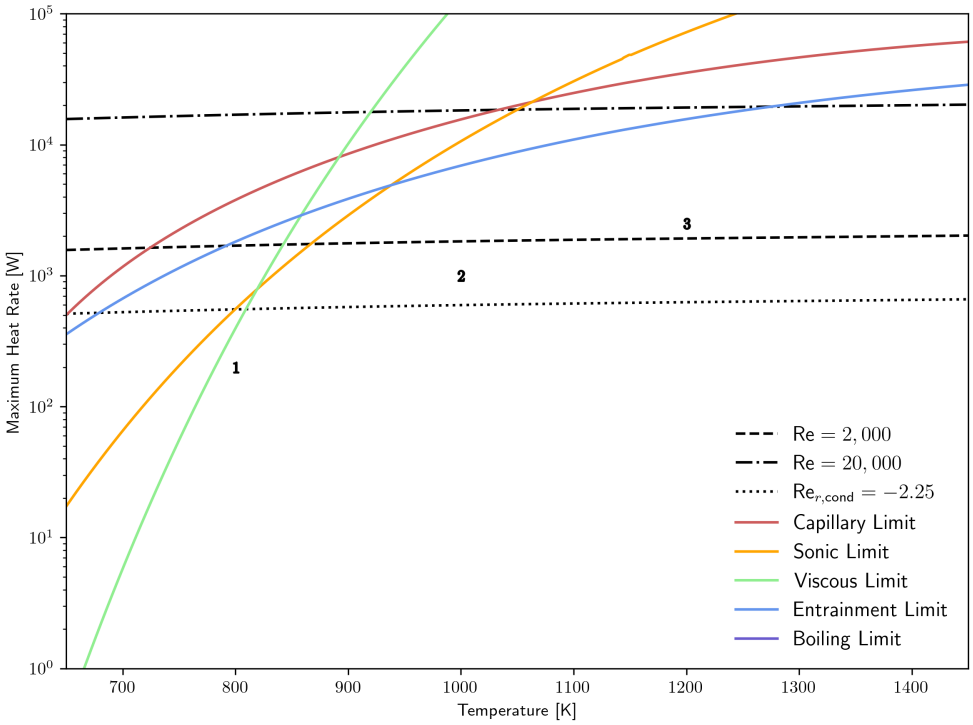

Figure 2: Test cases in heat pipe operating space.

Analytic solutions are generated with thermodynamic properties both from HTPIPE and Sockeye to illustrate differences arising from differences in properties. Vapor pressure drops are compared to analytic solutions from Busse [9] and Cotter [14]. Note that Cotter's theory usually picks either the inertial pressure drop or the viscous pressure drop, depending on the radial Reynolds number, but the solution shown here is the sum of both components. "Busse (Numerical Integration)" denotes the solution obtained by numerically integrating Busse's pressure gradient equation (Equation [18] in Reference [9]),

$$\frac{\mathrm{d}p_v}{\mathrm{d}x} = -\frac{4}{3}\rho_v \frac{\mathrm{d}}{\mathrm{d}x}\left[u_v^2\left(1-\frac{a}{6}+\frac{2a^2}{45}\right)\right] - 8\frac{\mu_v u_v}{R_v^2}\left(1+\frac{2}{3}a\right), \tag{65}$$

rather than using Busse's analytically integrated formulas. It was found that there was a significant discrepancy between the numerically-integrated solution and the analytic solution in the condenser (Equation [40] in Reference [9]). We were unable to produce an analytical solution for the pressure drop in the condenser that could be compared to Busse's solution, so we are not able to confirm if Busse's solution in the condenser has any mistake. As for the numerical integration performed here, there is high confidence, since the numerical integrations of the various pressure drop terms match the numerical pressure drop solution (compare the Δp_v and $\sum_i \Delta p_{v,i}$ sets in Figures 5, 9, and 12).

A vapor pressure drop "breakdown" plot is also presented, where the various contributions to the total pressure drop are estimated via numerical integration. The various terms are defined as follows:

$$\Delta p_v \equiv \int_0^x \frac{\mathrm{d}p_v}{\mathrm{d}x} dx', \tag{66}$$

$$\sum_i \Delta p_{v,i} \equiv \Delta p_{v,\text{visc}} + \Delta p_{v,\text{iner}} + \Delta p_{v,\text{iner-corr}} + \Delta p_{v,\text{vfgrad}} + \Delta p_{v,\text{vfgrad-int}}\,, \tag{67}$$

$$\Delta p_{v,\text{visc}} \equiv \int_0^x -\frac{f_v \rho_v |u_v| u_v}{2D_{h,v}} dx'\,, \tag{68}$$

$$\Delta p_{v,\text{iner}} \equiv \int_0^x -\frac{1}{\alpha_v}\frac{\mathrm{d}\alpha_v \rho_v u_v^2}{\mathrm{d}x} dx'\,, \tag{69}$$

$$\Delta p_{v,\text{iner-corr}} \equiv \int_0^x \frac{2(1-f_{\text{iner}})\Gamma_{\text{int}} u_v a_{\text{int}}}{\alpha_v} dx'\,, \tag{70}$$

$$\Delta p_{v,\text{vfgrad}} \equiv \int_0^x -\frac{p_v}{\alpha_v}\frac{\mathrm{d}\alpha_v}{\mathrm{d}x} dx'\,, \tag{71}$$

$$\Delta p_{v,\text{vfgrad-int}} \equiv \int_0^x \frac{p_{\text{int}}}{\alpha_v}\frac{\mathrm{d}\alpha_v}{\mathrm{d}x} dx'\,. \tag{72}$$

3.1 Case 1

This case is at a relatively low power and temperature; at this low power, Busse's theory can be applied, since the radial Reynolds number in the condenser is greater than -2.25. Sockeye was run with the second-order spatial discretization and compared to HTPIPE and analytic solutions.

Figure 3 shows the liquid pressure drop. The liquid pressure drop follows the analytic curve, other than oscillations that occur at the evaporator exit and condenser entrance, which are believed to be due to the sharp transitions in the heating profile at these positions. For example, the heat source is set to be uniform over the evaporator and immediately drop to zero in the adiabatic section. These oscillations can be remedied with more spatial refinement or smoother heating transitions. Also, the usage of TVD slope limiter schemes could help remedy these oscillations; however, more work is needed to prevent numerical artifacts in these schemes at the domain boundaries. Note that these oscillations do not appear to affect the total pressure drop, so their impact on the heat pipe performance is believed to be minimal. HTPIPE has a discrepancy because it approximates the annulus cross sectional area as $A_{\text{ann}} \approx \pi D_{\text{wick,i}} t_{\text{ann}}$ instead of using $A_{\text{ann}} = \frac{1}{4}\pi(D^2_{\text{clad,i}} - D^2_{\text{wick,o}})$, which under-approximates the area by 9.5%, which, because this area appears in the denominator of the pressure drop, over-approximates the pressure drop.

Figure 4 shows the vapor pressure drop. Two analytic theories are considered: Cotter's [14] and Busse's [9]. Busse's theory obtains the pressure drop as a function of position, giving the "Busse" sets, but, if the governing pressure gradient equation is instead integrated numerically, the "Busse (Numerical Integration)" set is obtained, which indicates a discrepancy with Busse's result in the condenser section. Sockeye's vapor pressure drop roughly follows "Busse (Numerical Integration)." For simplicity, Sockeye uses $a = 0$ in the adiabatic section and condenser, which is a source of some discrepancy. Also, the analytic solutions all assume uniform thermodynamic properties, whereas Sockeye's properties, such as density, vary along the heat pipe length.

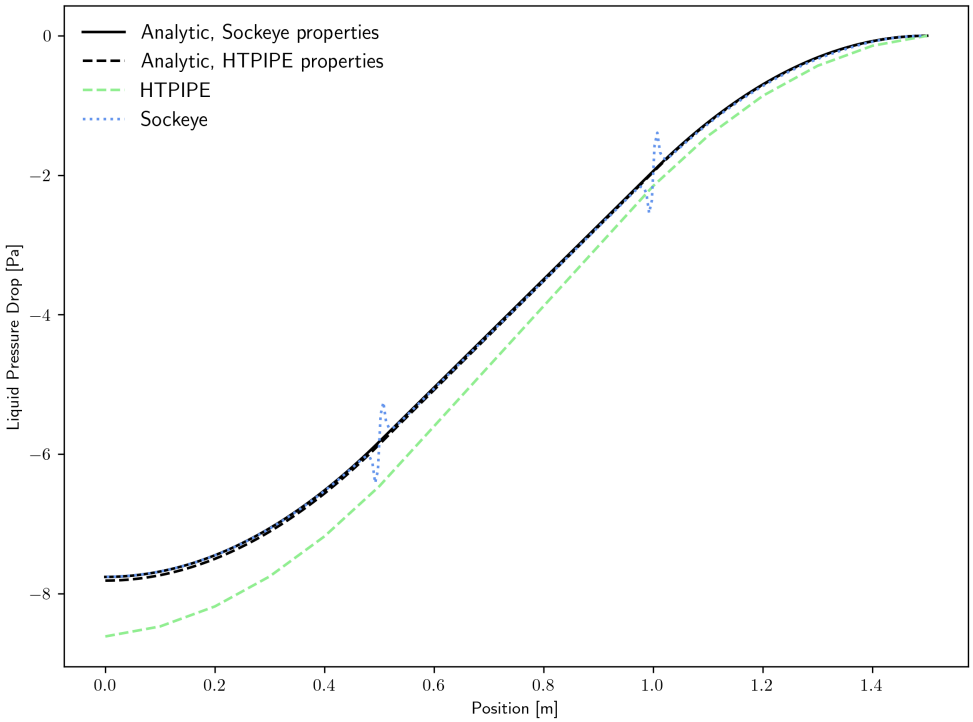

Figure 3: Case 1 liquid pressure drop.

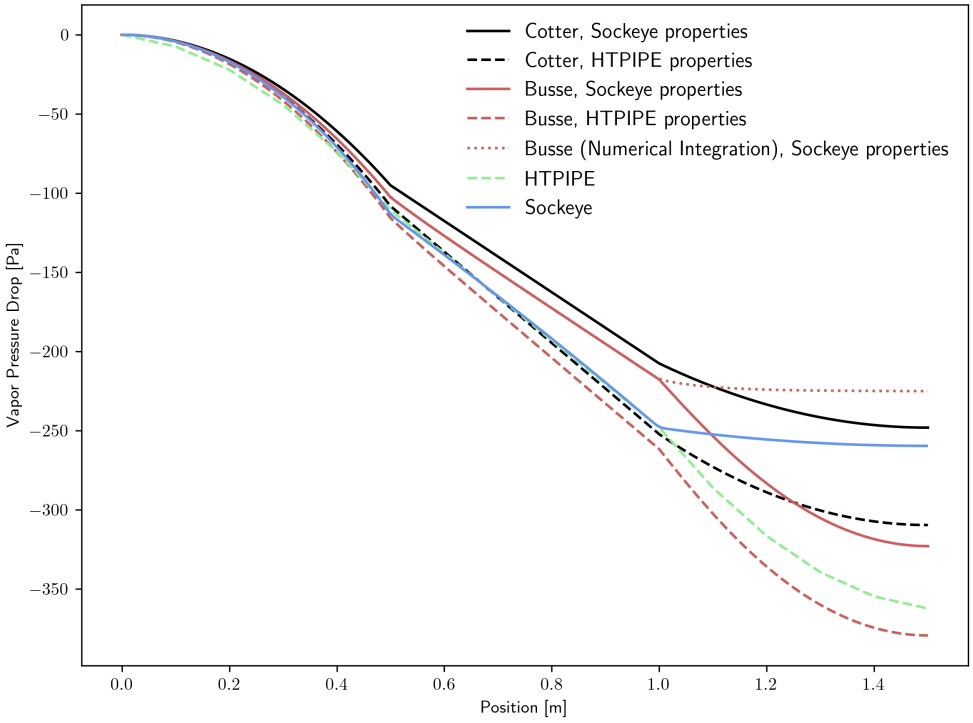

Figure 4: Case 1 vapor pressure drop.

Figure 5 shows Sockeye's vapor pressure drop breakdown. For this low power case, the viscous pressure drop is dominant over the inertial pressure drop. The inertial pressure drop cancels out over the length of the heat pipe, as expected.

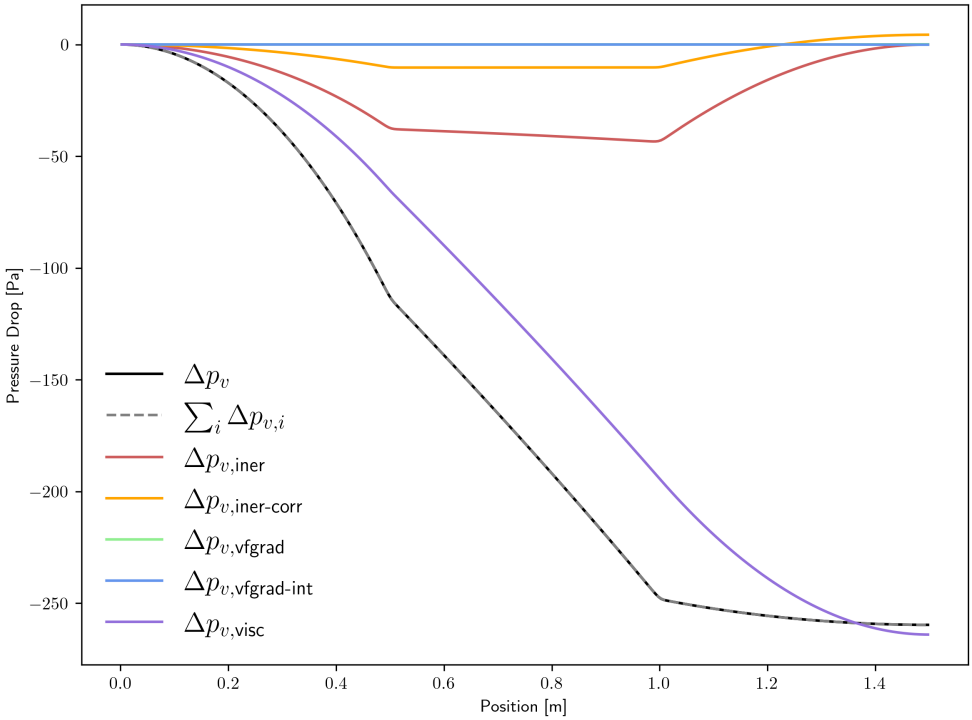

Figure 5: Case 1 vapor pressure drop breakdown.

Figure 6 shows the results of a spatial discretization study. The sets labeled "No Slope Reconstruction" correspond to Godunov's method, which is first-order accurate, and the sets labeled "Full Slope Reconstruction" correspond to the scheme resulting from using the piecewise-linear reconstruction of the solution as inputs to the numerical flux function, as discussed in Section 2.6. These results clearly show the excessive artificial dissipation resulting from the usage of the first-order-accurate scheme. This leads to significant jumps in the cell-average pressures, which can consequently cause an inaccurate capillary limit prediction. The second-order scheme still has some numerical artifacts at the interfaces between the evaporator, adiabatic, and condenser sections, due to the discontinuity in boundary conditions there. However, these artifacts are relatively small and disappear much more rapidly with mesh refinement than the pressure jumps in the first-order scheme.

3.2 Case 2

This case has an intermediate power, where the inertial pressure drop in the vapor phase becomes more significant. Again, the inertial pressure drop cancels out over the length of the heat pipe, but now the pressure profile shape is significantly different. Figures 7, 8, and 9 show the liquid pressure drop, vapor pressure drop, and vapor pressure drop breakdown results, respectively.

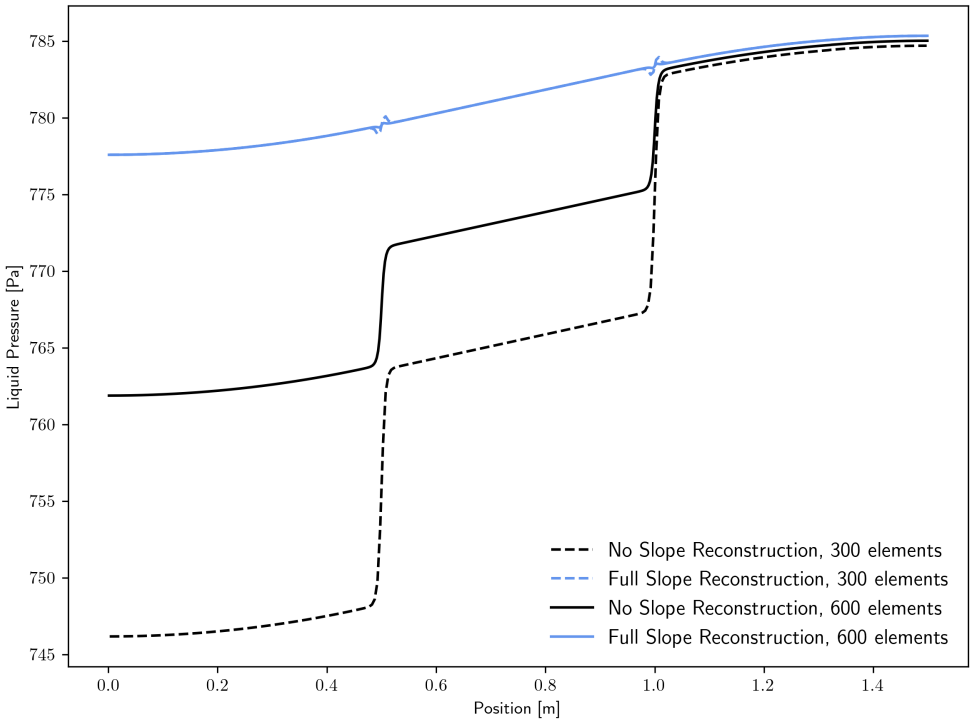

Figure 6: Comparison of spatial discretizations for Case 1.

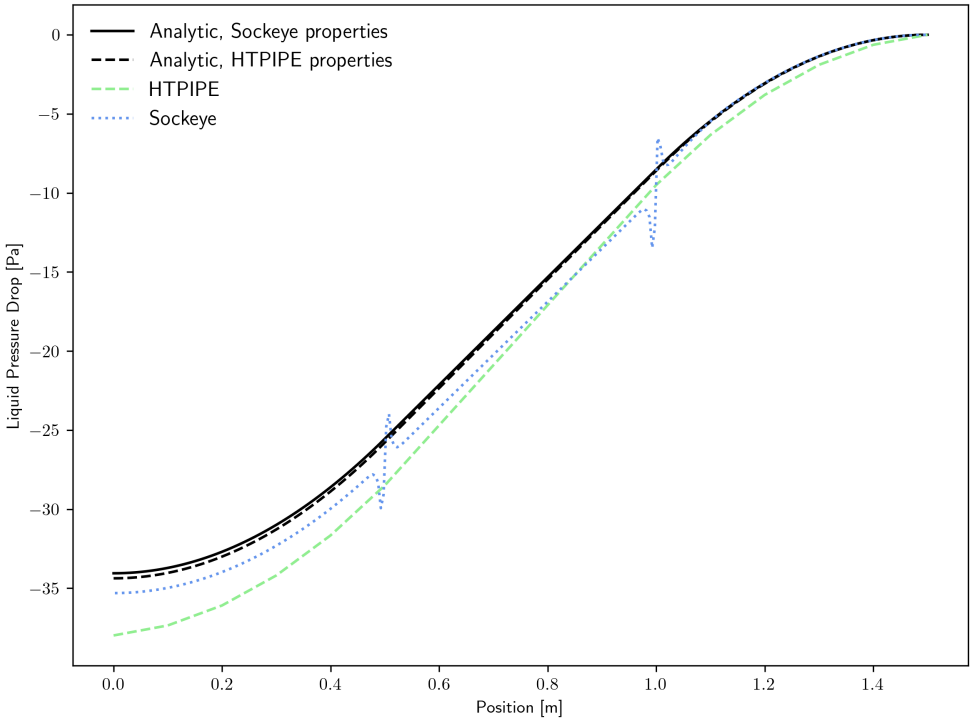

Figure 7: Case 2 liquid pressure drop.

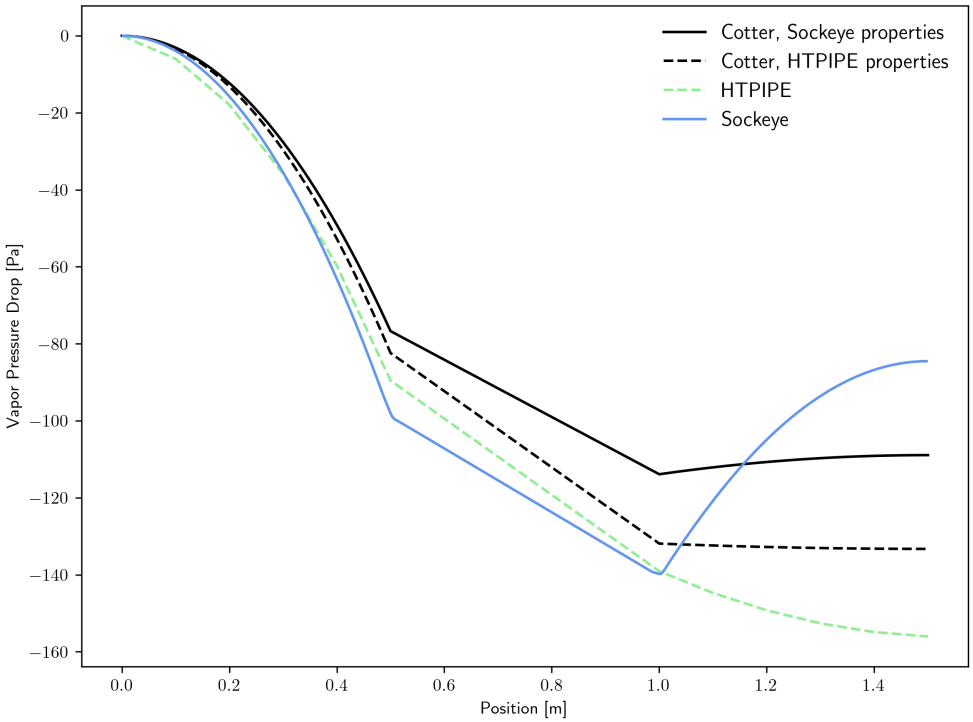

Figure 8: Case 2 vapor pressure drop.

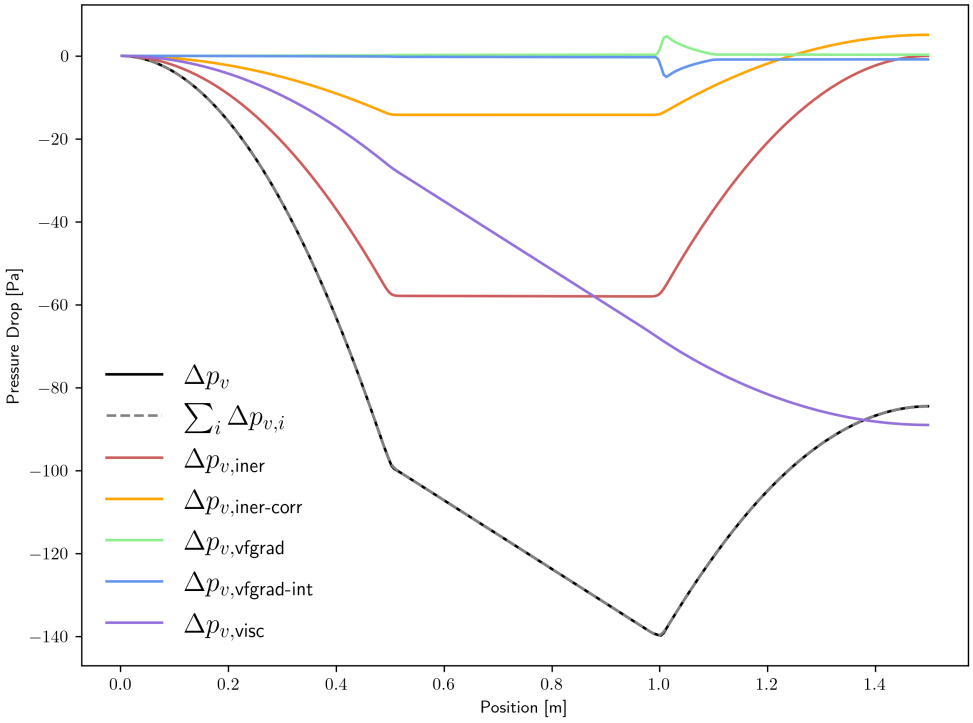

Figure 9: Case 2 vapor pressure drop breakdown.

3.3 Case 3

For the high-power case, inertial effects are most dominant. Now the volume fraction gradient becomes a bit more significant, particularly at the condenser entrance, and the volume fraction gradient terms are noticeable, although they tend to be roughly equal and opposite due to $p_v \approx p_{\text{int}}$. Figures 7, 8, and 9 show the liquid pressure drop, vapor pressure drop, and vapor pressure drop breakdown results, respectively.

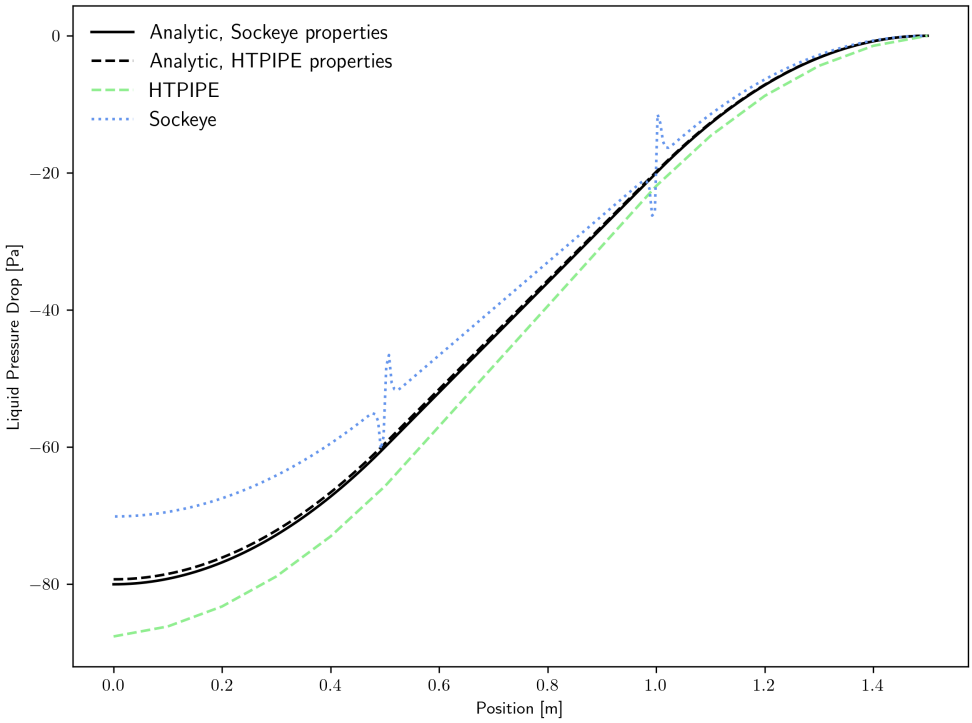

Figure 10: Case 3 liquid pressure drop.

4 CONCLUSIONS

We implemented several closure relations, including interfacial heat transfer coefficients, wall heat transfer coefficients, and friction factors, and developed a closures system to allow the easy switching of closure relations and allow the user to implement their own closures classes. Additionally, we implemented a second-order spatial discretization.

Three test cases at varying temperatures and power levels assessed the new closure relations in Sockeye against the steady-state heat pipe code HTPIPE, as well as analytic solutions. Comparisons showed good agreement for the liquid pressure drop. The vapor pressure drop had varied solutions for HTPIPE and the analytic solutions, and Sockeye produced total vapor pressure drops within the range of the other solutions. A spatial discretization study showed a significant advantage of the new, second-order scheme, which lacked the significant, nonphysical pressure jumps present in the first-order scheme. However, nonphysical oscillations in the solution were observed with the second-order scheme at the interfaces between the evaporator, adiabatic, and condenser regions.

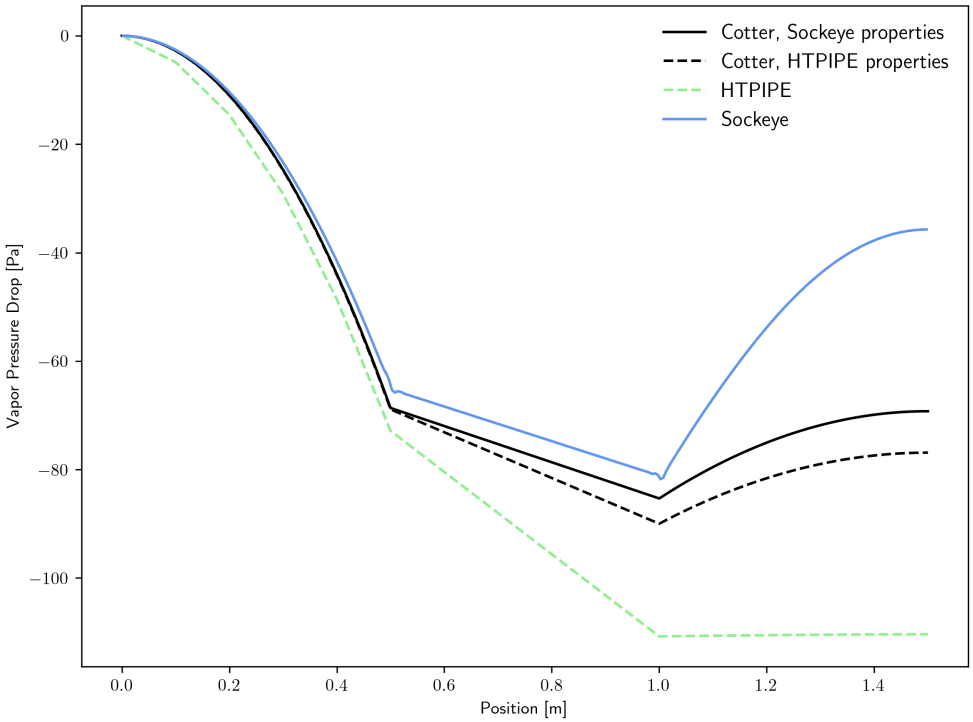

Figure 11: Case 3 vapor pressure drop.

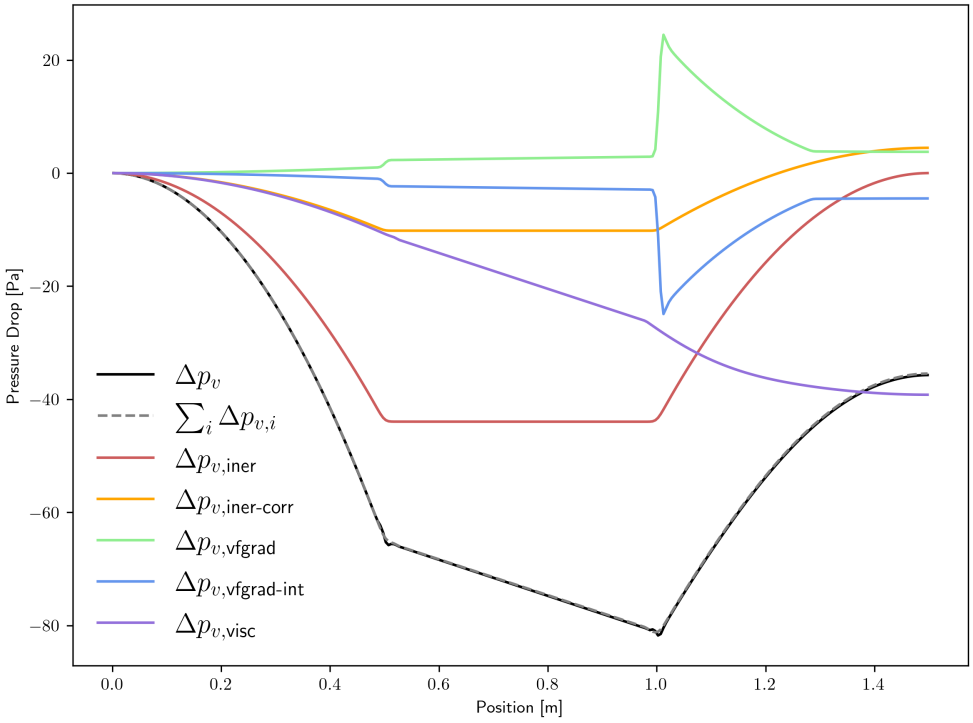

Figure 12: Case 3 vapor pressure drop breakdown.

Future work is needed to further assess Sockeye's closure relations. Analytic solutions employ restrictive assumptions, and the consequences of all of these assumptions and approximations may yield unrealistic reference solutions. Ultimately, experimental data is needed to assess these closures; however, a direct measurement of pressure drops inside of a heat pipe is needed but not easily obtained.

REFERENCES

[1] J. E. Hansel, R. A. Berry, D. Andrs, M. S. Kunick, and R. C. Martineau, "Sockeye: A 1-D, two-phase, compressible flow heat pipe application," *Nuclear Technology*, vol. 117, 2021.

[2] C. J. Permann, D. R. Gaston, D. Andrš, R. W. Carlsen, F. Kong, A. D. Lindsay, J. M. Miller, J. W. Peterson, A. E. Slaughter, R. H. Stogner, and R. C. Martineau, "MOOSE: Enabling massively parallel multiphysics simulation," *SoftwareX*, vol. 11, p. 100430, 2020.

[3] V. Carey, *Liquid-Vapor Phase-Change Phenomena: An Introduction to the Thermophysics of Vaporization and Condensation Processes in Heat Transfer Equipment*. CRC Press, third ed., 2020.

[4] A. Faghri, *Heat Pipe Science and Technology*. Global Digital Press, second ed., 2016.

[5] E. Skupinski, J. Tortel, and L. Vautrey, "Determination of convective coefficient for a sodium-potassium alloy in a circular tube," *International Journal of Heat and Mass Transfer*, vol. 8, pp. 937 – 951, 1965.

[6] M. Shah, "A survey of experimental heat transfer data for nucleate pool boiling of liquid metals and a new correlation," *International Journal of Heat and Fluid Flow*, vol. 13, no. 4, pp. 370 – 379, 1992.

[7] D. A. Reay, P. A. Kew, and R. J. McGlen, *Heat Pipes: Theory, Design and Applications*. Elsevier Ltd., sixth ed., 2014.

[8] K. A. Woloshun, M. A. Merrigan, and E. D. Best, "HTPIPE: A steady-state heat pipe analysis program: A user's manual," Tech. Rep. LA-11324-M, Los Alamos National Laboratory, 11 1988.

[9] C. A. Busse, "Pressure drop in the vapor phase of long heat pipes," in *Proceedings of IEEE Conference of Thermionic Conversion Specialists*, (Palo Alto, CA), pp. 391–398, 1967.

[10] F. M. White and H. Xue, *Fluid Mechanics*. New York, NY: McGraw-Hill, ninth ed., 2021.

[11] N. M. Natarajan and S. M. Lakshmanan, "Laminar flow through annuli: Analytical method of pressure drop," *Indian Chemical Engineer*, vol. 5, no. 3, pp. 50–53, 1973.

[12] D. Furfaro and R. Saurel, "A simple HLLC-type Riemann solver for compressible non-equilibrium two-phase flows," *Computers & Fluids*, vol. 111, pp. 159–178, 2015.

[13] E. Toro, *Riemann Solvers and Numerical Methods for Fluid Dynamics: A Practical Introduction*. Springer Berlin Heidelberg, 2009.

[14] T. Cotter, "Theory of heat pipes," Tech. Rep. LA-3246-MS, Los Alamos National Laboratory, 1965.